An MO-Theoretical Treatment of the Cationic Ring-Opening Polymerisation. I. Ethylene Oxide

Gernot FRENKING, Hiroshi KATO,* and Kenichi FUKUI

Department of Hydrocarbon Chemistry, Faculty of Engineering, Kyoto University, Sakyo-ku, Kyoto 606
**College of General Education, Nagoya University, Chikusa-ku, Nagoya 464*

(Received July 26, 1974)

The stereochemical course of the acid-catalyzed ring-opening polymerisation of ethylene oxide (e.o.) has been investigated on the basis of the CNDO/2 method. By the calculation of the total energy of the interacting system of e.o. and protonated e.o. the most favored reaction path is indicated. The activation energy is found to consist only of the desolvation process. The effect of the deformation of the molecular geometry upon the net charge, the total energy, and the shape of particular MO's is discussed. It is concluded that the ring strain does not influence the rate. By means of configuration analysis, the dominance of the HOMO–LUMO interaction in the later stage of the reaction has been established. The initiation and propagation reactions follow the same reaction mechanism.

Extensive experimental studies in the field of ring-opening polymerisation (ROP) have been made.[1] In contrast to numerous papers reporting those results, however, there have been very few theoretical treatments of this field.[2] The experimental results concerning the reaction path of the acid-catalyzed ROP of cyclic ethers can be summarized as follows:[3] The initiator is first formed by a reversible protonation:

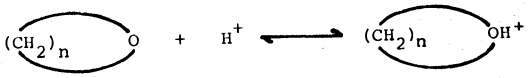

The initiation is considered to be the addition of a monomer to this protonated monomer. There is much evidence that the process of the ring-opening addition takes place as an S_N2-like backside attack. The propagation step is essentially constructed by a succession of similar processes at the terminal monomeric unit of a polymer chain:

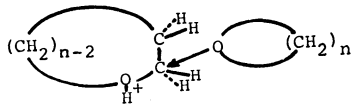

The backside attack is indicated by an inversion at the attacked carbon atom. However, still remains some doubt about the sequence of the bond interchange and the transition state. There has been discussed a "borderline S_N2-mechanism,"[4] where the old C–O bond is already partly broken at a rather early stage of the attack. Recent kinetic studies of the cationic ROP of some four-membered cyclic ethers show that the entropy of activation is the dominating factor in the reactivity.[5]

In the present and forthcoming papers, we want to report the results of our MO-theoretical treatment of various aspects of the reactivity and stereochemistry of heterocyclic-ring compounds in ROP. We start with ethylene oxide (e.o.), since it may serve as a simple model case for other, more complicated compounds.[6] Using the CNDO/2 method, we treat the isolated e.o. and its protonated compound, and also their interacting system. In order to determine the most favored geometries and reaction path, we examine the effect of changes in several geometrical parameters. Furthermore, utilizing the frontier theory[8] and configuration analysis,[9] the mechanisms of cationic ROP are investigated.

Calculations and Used Geometries

All our MO-calculations were based upon the CNDO/2 model of Pople *et al.*[7]

Figure 1(a) shows the energy levels of the MO's of e.o. and protonated e.o., together with the chosen geometry. Figure 1(b) shows the resulting net charges.

We calculated the total energy of the combined system of e.o. and protonated e.o. with different geometries. Figure 2 shows the geometries which gave the energy minimum at the fixed C–O′ distance for each of the frontside and backside attacks.[16] Further-

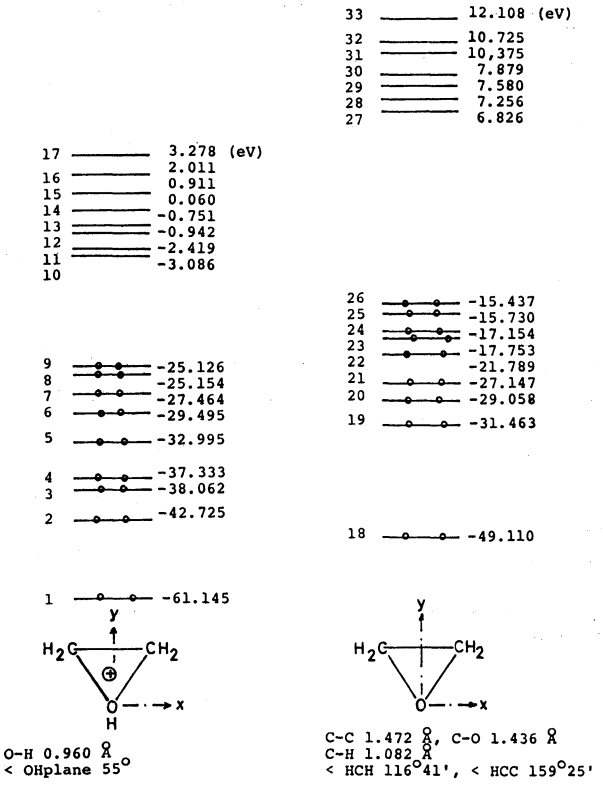

Fig. 1(a). MO energy levels and geometry of ethylene oxide and protonated ethylene oxide.

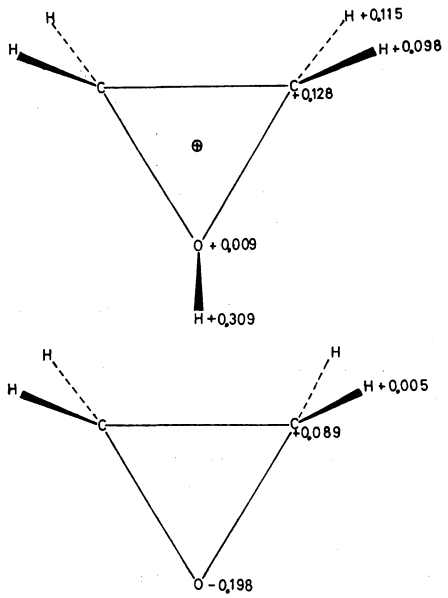

Fig. 1(b). Net charges of ethylene oxide and protonated ethylene oxide.

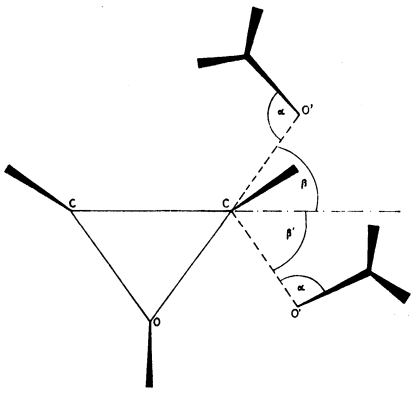

Fig. 2. Geometry of the molecules in the two attacking directions, the backside attack upper and the frontside attack lower.
$\alpha=110°$, $\beta=60°$, $\beta'=60°$.

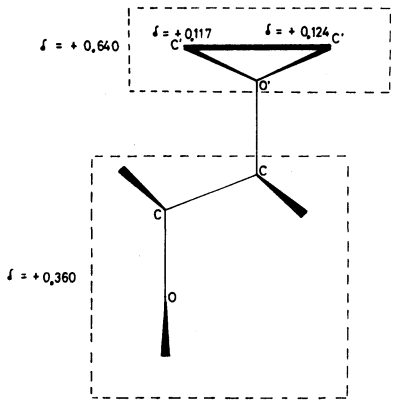

Fig. 3. Geometry of the final product of the initiation reaction and net charge distribution. The ring has the same geometry as e.o. (see Fig. 1).
O'–C 1.430 Å; C–C 1.540 Å; C–O 1.430 Å; C–H 1.090 Å; O–H 0.960 Å; $<$O'CC 110°; $<$HC plane $=<$OC plane 55°.

Table 1. Values of total energy, energy between the attacking oxygen (O') and the attacked carbon (C), and the net charge transfer with different geometries

$r_{C-O'}$ [Å]	Stretching of r_{C-O} [Å]	Bending of C–H bond γ [degree]	E_{tot} [a.u.]	$E_{C-O'}$ [a.u.]	Transferred charge
		Attack along the y-axis			
2.5	0	0	−71.8140	−0.013	0.002
		$\beta=60°$ (backside attack)			
2.5	0	0	−71.8068	−0.012	0.005
		−30	−71.8100	−0.019	0.009
	0.2	0	−71.7529	−0.018	0.012
		−60	−71.7463	−0.032	0.019
2.0	0	0	−71.8114	−0.064	0.047
		−30	−71.8302	−0.104	0.061
		−60	−71.8017	−0.134	0.084
	0.2	0	−71.7709	−0.095	0.083
		−30	−71.8031	−0.140	0.095
		−60	−71.7962	−0.177	0.125
1.5	0	0	−71.7323	−0.341	0.246
		−30	−71.8262	−0.462	0.290
		−60	−71.8528	−0.548	0.352
	0.2	0	−71.7412	−0.434	0.354
		−30	−71.8445	−0.546	0.376
		−60	−71.8951	−0.632	0.424
		$\beta'=60°$ (frontside attack)			
2.5	0	0	−71.8146	−0.019	0.009
	0.2	0	−71.7583	−0.027	0.012
		30	−71.7185	−0.026	0.014
2.0	0	0	−71.8245	−0.094	0.048
		30	−71.7973	−0.099	0.052
	0.2	0	−71.7880	−0.151	0.089
		30	−71.7561	−0.161	0.109
1.5	0	0	−71.7833	−0.493	0.250
		30	−71.7929	−0.538	0.285
	0.2	0	−71.8460	−0.645	0.408
		30	−71.8595	−0.697	0.451
		final product of the initiation reaction			
			−71.9441	−0.890	0.640

more, the neutral e.o. has been placed in a planar and perpendicular position to the protonated e.o. plane. Among all of these calculations, the geometries adapted in Fig. 2 gave the lowest energy values with regard to the above-mentioned parameters (see Table 1).

In the next step, we examine the energy minimum as to the attacking direction with the two C–O' distances of 2.0 and 2.5 Å. We also calculate the energy of the final product of this reaction of ROP. Its geometry is shown in Fig. 3, while the resulting energy is listed in Table 1.

Finally, we investigate the deformation of the ring of protonated e.o., since the geometry of the attacked protonated e.o. changes toward the geometry of the final product throughout the reaction. The considered deformations are indicated in Fig. 4, where the deformations of 1 and/or 4 are taken in the frontside attack course and those of 2, 3, and/or 4 for the backside attack.

The results are listed in Table 1. The table also

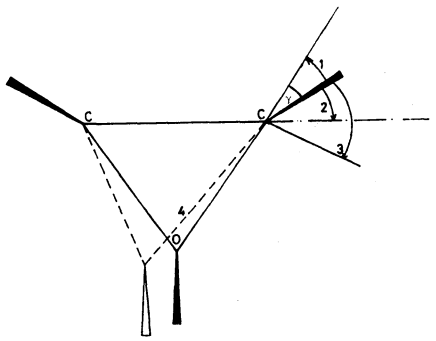

Fig. 4. Assumed deformations of the protonated ethylene oxide during the attack of the neutral molecule.
1: Hydrogens shifted up to $\gamma=30°$
2: Hydrogens shifted down to $\gamma=-30°$
3: Hydrogens shifted down to $\gamma=-60°$
4: One C–O bond length stretched by 0.2 Å.

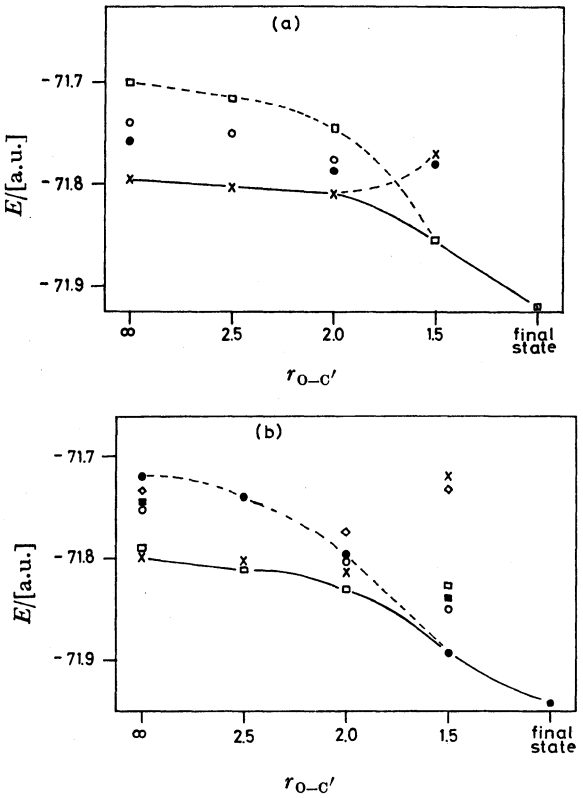

Fig. 5. The changes of energy levels along the two paths of attacking with the change of geometry indicated.
(a): Frontside attack
C–O bond length normal γ: 0° (×), γ: 30° (●)
C–O bond length +0.2 Å δ: 0° (○), δ: 30° (□)
(b): Backside attack
C–O bond length normal γ: 0° (×), γ: −30° (□), γ: −60° (○).
C–O bond length +0.2 Å γ: 0° (◇), γ: −30° (■), γ:−60° (●).

gives the values of the transferred charge from the neutral to the protonated compound and the values of the energy of the C–O′ bonding (E_{AB} in CNDO/2). Figures 5(a) and 5(b) show the total energies in relation to the C–O′ distance. The datum for $r=\infty$ is the simple sum of the values for the separated molecules.

Discussion

In spite of the use of many approximations, the results give interesting insights into the reaction path. Comparing the frontside and the backside attacks with the energy values shown in Fig. 5(a) and 5(b), it can be seen that there is not much difference with $r_{C-O'}$ values larger than 2.0 Å. After this stage, the backside attack is strongly favored from an energetic point of view.

It has been proposed in several papers by Fukui *et al.*[8] that "a majority of chemical reactions should take place at the position and in the direction of the maximum overlapping of the HOMO (Highest Occupied MO's) and the LUMO (Lowest Unoccupied MO's)." The HOMO of e.o., which is not shown here, is indeed mainly localized on the lone-pair oxygen p_z orbital (AO coefficient 0.88). There are two nearly degenerated LUMO's of the protonated e.o. (a' at −3.086 eV and a'' at −2.419 eV, with the point group C_s). They correspond to the a_1 and b_2 LUMO's of e.o. (point group C_{2v}). The consideration of both of them has previously been emphasized in the calculations of the anionic ROP of e.o.[10] The shapes of

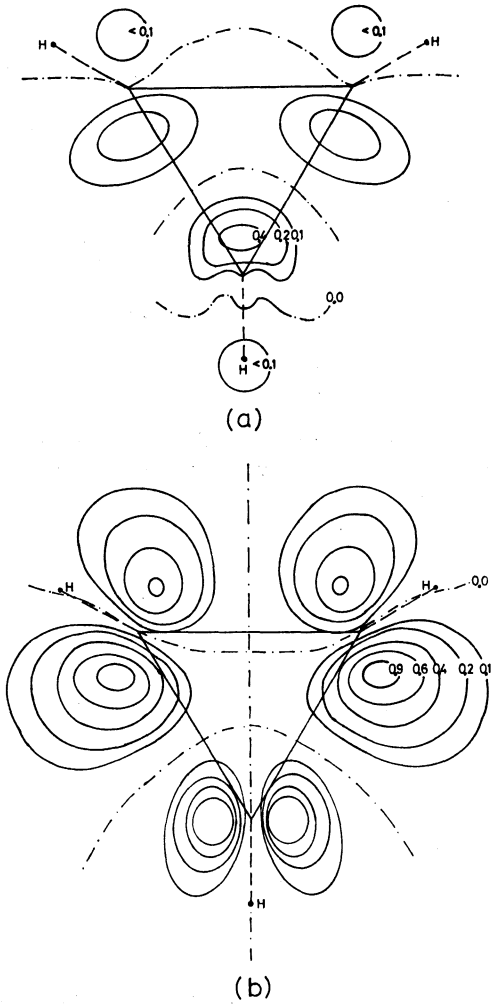

Fig. 6. The LUMO's of protonated e.o. The figures indicate the values of the real MO's in the molecular plane. The contour lines correspond to the density values indicated.
(a): a' LUMO (b): a'' LUMO

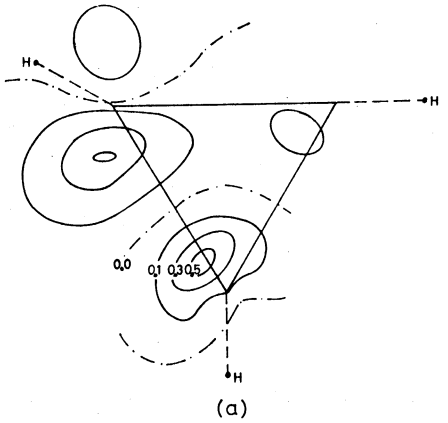

(a)

(a): a' LUMO at normal C–O bond length, H-shift with $\gamma=-30°$.

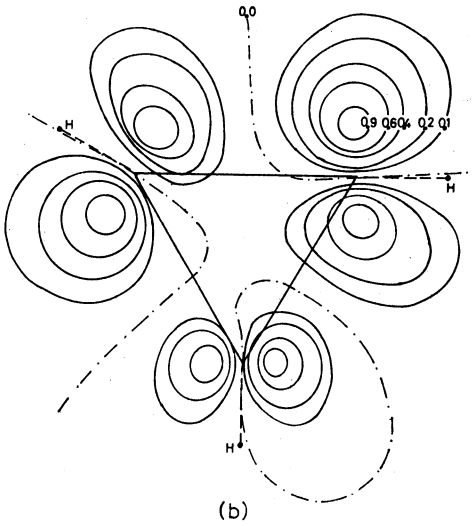

(b)

(b): a'' LUMO at normal C–O bond length, H-shift with $\gamma=-30°$.

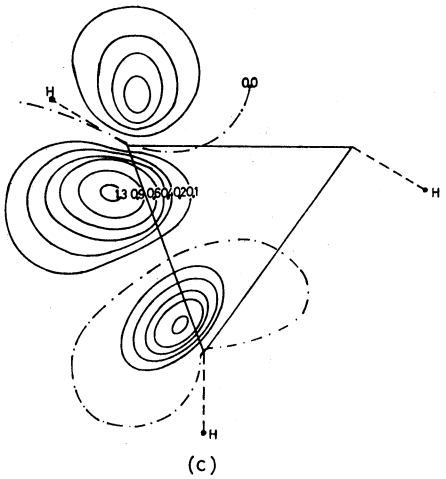

(c)

(c): a' LUMO at C–O bond length $+0.2$ Å, H-shift with $\gamma=-60°$.

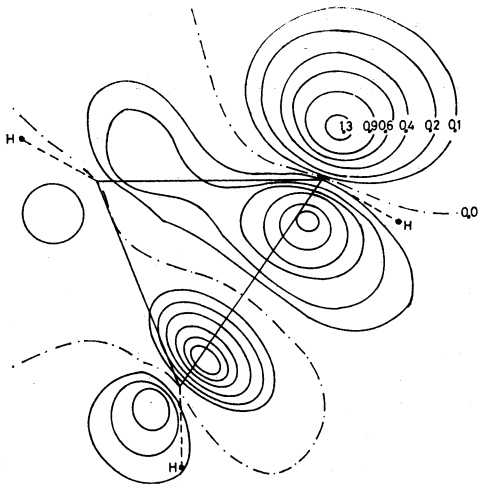

(d)

(d): a'' LUMO at C–O bond length $+0.2$ Å, H-shift with $\gamma=-60°$.

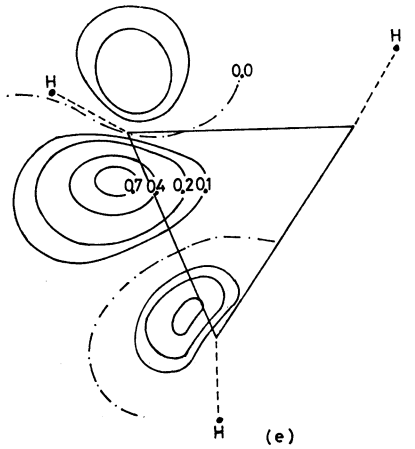

(e)

(e): a' LUMO at C–O bond length $+0.2$ Å, H-shift with $\gamma=30°$.

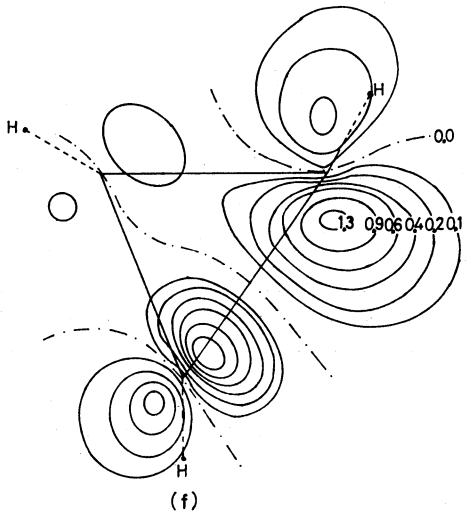

(f)

(f): a'' LUMO at C–O bond length $\times 0.2$ Å, H-shift with $\gamma=30°$.

Fig. 7. Change of the two LUMO's under some deformations of the geometry of protonated e.o.

these LUMO's in the molecular plane are shown in Figs. 6(a) and 6(b). Both of them have a node between oxygen and carbon, but the a' LUMO has its main extension in an antibonding region between oxygen and hydrogen. (In Fig. 6(a) the contour lines not on the molecular plane do not appear.) Therefore, it may be presumed that it is the a'' LUMO which plays the dominant role in the ring cleavage.

This LUMO mainly extends in the initial geometry at the frontside. However, it is noticed that the shapes and energies of these LUMO's may vary with the geometry. Figures 7(a)—(f) collect the shapes of the LUMO's with various geometries which give the local minima for the respective $r_{C-O'}$ values, as given in Table 1. With these geometries, the notations a' and a'' lose their exact meaning because of the loss of symmetry, but they are still kept for the sake of convenience. Figure 7(b) clearly indicates that the shift of the hydrogens, which is expected to occur at an earlier stage of the reaction, as is shown in Table 1 and Fig. 5, results in a reversal of the maximum extension of the a'' LUMO from the frontside to the backside direction, whereas the extension of the a' LUMO at the attacked carbon atom is reduced. This tendency is even more accelerated with the deformation of the ring frame and a further hydrogen shift, as is shown in Figs. 7(c) and 7(d). Figures 7(e) and 7(f) show a similar trend for the frontside reaction.

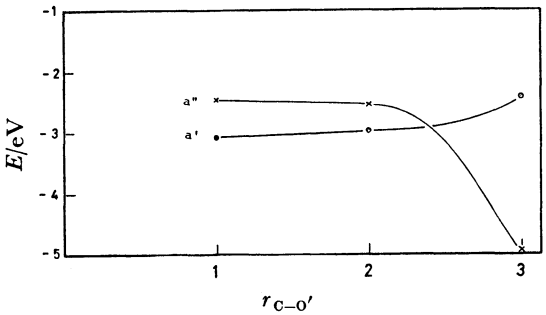

Fig. 8. Change of the energy level of the two LUMO's of protonated e.o. with some deformations which correspond to the reaction path of the backside attack (see Fig. 5(b)).
1: initial geometry, 2: C–O bond length normal, H-shift γ −30°, 3: C–O bond length +0.2 Å, H-shift γ −60°.

That it is the a'' LUMO and not the a' LUMO which is dominating in the HOMO–LUMO interaction can also be seen from the change in the energy level along with the change in the geometry, as is indicated for the backside attack in Fig. 8. The narrowing of the frontier orbitals has already been pointed out by Fukui *et al.*[8]

Some additional calculations have been carried out for the backside attack. We calculated the composed system by placing the neutral e.o. at a $r_{C-O'}$ distance of 2.5 Å along the y-axis in a planar arrangement to the protonated compound, as the Coulomb attraction should be the dominating force in this case. The numerical results, given in Table 1, show a greater stabilisation than the corresponding value for the assumed backside path. Furthermore, we varied the geometry parameters with a $r_{C-O'}$ distance of 1.5 Å. The values for β (see Fig. 2) have been taken as 75 and 45°, and the hydrogen shift with $\gamma=-45°$ (see Fig. 4). However, all these calculations gave no further stabilisation compared to the values for $\beta=60°$ and $\gamma=-60°$ (see Table 1). As our results for the principal reaction mechanism are independent of the exact location, we did not make any further calculations concerning the exact reaction path.

Additional information is given by the results of the configuration analysis[9,11] listed in Table 2, where some absolute values of coefficients for the ground state, monotransferred (delocalized), and intramolecular monoexcited (polarized) configurations are presented. The large value of the coefficient of the ground-state configuration at the early stage of the reaction indicates the dominance of the Coulomb interaction. However, the dramatically increasing value of the monotransferred configuration at $r_{C-O'}=1.5$ Å, especially that corresponding to the transfer from of e.o. the HOMO to the LUMO of protonated e.o.,[12] shows the importance of this kind of interaction at the final stage of the reaction.

From Table 1 it can be seen that the values for $E_{C-O'}$ and the quantities of charge transfer show no remarkable parallelism with the total energy, nor is there any interdependence between them. Roughly speaking, both values increase with the lowering of the total energy. It is interesting that, with the distance $r_{C-O'}$ of 1.5 Å, the backside attack shows a significantly lower total energy, but smaller $E_{C-O'}$ and transferred charge, than the frontside attack.

It is worthwhile to examine the charge transfer in more detail. Table 3 shows the change in the net charge of each atom at the different reaction stages for the local minimum energy (see Fig. 5). The numbers represent the differences from the net charge calculated for the isolated molecules with the respective geometry, where the + sign refers to the decrease in the atomic electron density caused by the interaction, and the − sign, to its increase. In contradiction to the whole protonated e.o. molecule coming more negative (less positive), the attacked carbon atom, 2, be-

Table 2. Absolute values of the coeeficients for the ground state, some monotransferred and monoexcited configurations along the backside and frontside paths only the one or two largest values are indicated

Attacking-direction	$r_{C-O'}$ [Å]	Ψ_0	Coefficients for monotransferred configurations	Coefficients for monoexcited configurations
Backside ($\beta=60°$)	2.5	0.999	$0.06(\Psi_{26\to11})$; $0.03(\Psi_{21\to11})$	$0.02(\Psi_{24\to27})$
	2.0	0.960	$0.17(\Psi_{36\to11})$; $0.08(\Psi_{21\to11})$	$0.03(\Psi_{6\to11})$; $0.03(\Psi_{23\to27})$
	1.5	0.690	$0.39(\Psi_{26\to10})$; $0.18(\Psi_{21\to10})$	$0.19(\Psi_{8\to10})$; $0.13(\Psi_{5\to10})$
Frontside ($\beta'=60°$)	2.5	0.992	$0.04(\Psi_{36\to11})$; $0.04(\Psi_{26\to10})$	$0.03(\Psi_{23\to27})$
	2.0	0.959	$0.13(\Psi_{36\to11})$; $0.07(\Psi_{26\to10})$	$0.04(\Psi_{23\to27})$
	1.5	0.598	$0.39(\Psi_{36\to10})$; $0.18(\Psi_{21\to10})$	$0.33(\Psi_{9\to10})$; $0.14(\Psi_{5\to10})$

TABLE 3. DIFFERENCE OF THE NET CHARGES AT EACH ATOM BETWEEN THE COMBINED SYSTEM AND ISOLATED MOLECULES WITH THE RESPECTIVE GEOMETRY. THE GEOMETRIES ARE THOSE ONES WHICH GAVE MINIMA IN THE ENERGY CALCULATIONS (see Table 1)

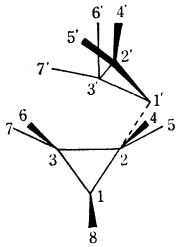

Atom	$r_{C-O'}$=2.5Å	$r_{C-O'}$=2.0Å	$r_{C-O'}$=1.5Å
1	−0.007	−0.029	−0.128
2	+0.011	+0.042	+0.084
3	−0.004	−0.021	−0.094
4	+0.003	−0.008	−0.064
5	+0.002	−0.010	−0.066
6	−0.004	−0.011	−0.046
7	−0.004	−0.010	−0.043
8	−0.003	−0.013	−0.073
1′	−0.027	−0.018	+0.132
2′	+0.003	+0.006	+0.021
3′	+0.003	+0.005	+0.020
4′	+0.030	+0.042	+0.079
5′	−0.014	−0.007	+0.046
6′	+0.030	+0.042	+0.079
7′	−0.015	−0.008	+0.045

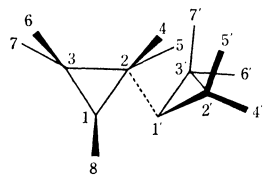

1	+0.003	−0.014	−0.173
2	+0.014	+0.061	+0.184
3	−0.010	−0.037	−0.102
4	−0.006	−0.017	−0.084
5	−0.007	−0.019	−0.056
6	−0.004	−0.009	−0.035
7	−0.005	−0.011	−0.100
8	+0.005	−0.001	−0.086
1′	−0.058	−0.053	+0.160
2′	+0.009	+0.011	+0.016
3′	+0.001	0.0	+0.008
4′	+0.030	+0.039	+0.080
5′	−0.001	+0.007	+0.055
6′	+0.030	+0.038	+0.078
7′	−0.003	+0.006	+0.054

comes more positive. Similarly, the oxygen atom, 1′, of the neutral molecule is still at $r_{C-O'}$=2.0 Å, more negative than in the isolated molecule, before it becomes more positive at $r_{C-O'}$=1.5 Å.

The potential curve of the reaction path anticipated from Fig. 5 indicates the absence of an energy barrier. This can easily be understood in view of the important role played by the solvent in ionic reactions. It has been found that this is particularly important for the reactivity of cyclic ethers in ROP.[13] Polar solvents stabilizing the monomers much better bring about a remarkable decrease in the reactivity of the monomers in ROP, compared with less polar solvents. Our calculations indicate that the activation energy originates only from the desolvation process. Therefore, the location of the transition state along the reaction path of Fig. 5(a) remains rather uncertain, however, the facts that the deformation of the ring frame occurs rather late ($r_{C-O'}$ <2.0 Å) and is accompanied by a rapid decrease in the total energy suggest that the transition state is placed somewhere earlier, with a geometry where the ring frame of the protonated e.o. is not yet deformed. If this is true, it follows that, in kinetically-controlled reactions where the activation energy determines the reaction rate, the ring strain is not influential on the rate. This has already been pointed out by Saegusa *et al.*[14] in reporting on their kinetic studies of 4-, 5-, and 7-membered cyclic ethers in cationic ROP. They found that the activation entropy is the most important factor in determining the reactivity.

There remains one problem. So far we have dealt only with the initiation step, but it has been stressed that the propagation step is quite different in its reaction rate, the latter being faster than the former.[15] The difference is as follows: in the propagation step, e.o. attacks an oxyethylated e.o. cation instead of a protonated one, and the length of the substituent chain is supposed to be not very important in connection with the reaction rate. Accordingly, we calculated the LUMO of the product of the initiation step. Figure 9 shows its shape in the ring plane. As the AO coefficients of this MO at atoms not placed in the ring plane are smaller than 0.03, it can be thought that the charges are located only in this plane. A comparison with the a'' LUMO of the protonated e.o. (Fig. 6(b)) shows a great similarity. In the case of alkylated e.o., however, the LUMO is not degenerated, being the lowest one not undergoing deformation due to the interaction. Also, the charge distributions (Fig. 3) of

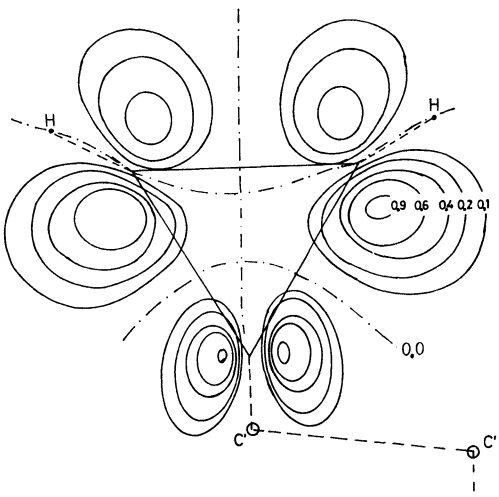

Fig. 9. The LUMO of the final product of the initiation reaction with the geometry of Fig. 3, indicating the values in the ring plane.

the atoms located at the ring are nearly the same as those of the protonated e.o. (Fig. 1(b)). From those facts, it can be expected that the mechanisms of the propagation reaction is not very different from the initiation.

The question is left why the rate of the propagation reaction is higher than the initiation reaction. The orbital energies of the LUMO's of the respective cations lead us to the opposite results. The LUMO of protonated e.o. (−3.086 eV) is lower than the LUMO of the oxyethylated e.o. (−1.629 eV). However, our results have shown that the bond breaking is more important than the bond making. The E_{AB} values for the C–O bond which is going to break during the reaction indicate a weaker bond for the oxyethylated e.o. (−0.816 eV) than for the protonated e.o. (−0.829 eV). This gives an explanation of the difference in the reaction rate.

From these calculations, the stereochemical course can be summarized as follows: the attack of the e.o. starts along the y-axis and is, in the beginning, governed by the Coulomb attraction only. The approach toward one carbon atom is accompanied by a shift of the connected hydrogens at a rather early stage of the reaction and produces a change in the a'' LUMO extension towards the attacking oxygen. This in turn accelerates the reaction by an increase in the charge transfer resulting from better HOMO–LUMO interaction. The deformation of the ring frame at a later stage accelerates this process still more and causes remarkable decreases in the total energy and also the C_2–O_1 bonding energy and increases in the amount of charge transfer and the C–O′ bonding energy. In this way, the deformation of the protonated compound leads to a reaction path with a lower energy for the backside attack than for the frontside attack.

One of the authors (G.F.) wishes to express his gratitude to Professor Takeo Saegusa and Dr. Shiro Kobayashi for a valuable discussion; he is also indebted to Dr. Hiroshi Fujimoto, Mr. Satoshi Inagaki, Mr. Tsutomu Minato, and Mr. Shigeki Kato for making avalaible the computer programs.

All three authors wish to express their appreciation to the Data Processing Center of Kyoto University for the generous permission to use the FACOM 230-60 computer there.

Thank is given to the Japanese Minister of Education and the Deutscher Akademischer Austauschdienst for giving grant to one of the authors (G.F.).

References

1) a) R. E. Parker and N. S. Isaacs, *Chem. Rev.*, **59**, 737 (1959); b) Y. Ishii and S. Sakai, "Ring Opening Polymerisation," ed. by K. C. Frisch and S. L. Reegen, Marcel Dekker, (1969), pp. 13—109.

2) K. Fukui, H. Kato, T. Yonezawa, and S. Okamura, This Bulletin, **37**, 904 (1964).

3) See Ref. 1b), p. 16.

4) See Ref. 1a), p. 746.

5) T. Saegusa and S. Kobayashi, *Progr. Polym. Sci.*, **6**, 107 (1973).

6) a) J. Koskikallio and E. Whalley, *Trans. Faraday. Soc.*, **59**, 815 (1959); b) C. C. Price and R. Spector, *J. Amer. Chem. Soc.*, **88**, 4171 (1966).

7) J. A. Pople, D. P. Santry, and G. A. Segal, *J. Chem. Phys.*, **43**, 129 (1965).

8) See *e.g.* K. Fukui, *Fortschr. Chem. Forsch.*, **15**, 1 (1970) and literatures cited therein.

9) See *e.g.* H. Baba, S. Suzuki, and T. Takemura, *J. Chem. Phys.*, **50**, 2028 (1969); H. Fujimoto, S. Kato, S. Yamabe, and K. Fukui, *ibid.*, **60**, 572 (1974).

10) H. Fujimoto, M. Katata, S. Yamabe, and K. Fukui, This Bulletin, **45**, 1320 (1971); note the choice of a different principal axis in the determination of the symmetry group.

11) S. Yamabe, T. Minato, H. Fujimoto, and K. Fukui, *Theor. Chim. Acta*, **32**, 187 (1974).

12) The reader is reminded that the succession of the orbitals denoted for the initial geometry in Fig. 1(a) changes in part because of the change in geometry. Therefore, the a'' LUMO of the protonated e.o., which plays the dominating part in the HOMO–LUMO interaction, is (in the succession of Fig. 1(a)) in the beginning the 11, but later the 10. See also Fig. 8.

13) See Ref. 5, p. 114, Table 1.

14) See Ref. 5, p. 145, Table 8.

15) See Ref. 5, p. 129.

16) The calculations where geometrical data are not listed have been carried out for the C–O′ distance of 1.5 Å and for the values for $\beta=30$, 60, 90°; $\beta'=30$, 60, and 90°, where β refers to the angle of backside attack, and β', to the frontside attack, as is indicated in Fig. 2.